Biofilm 9 (2025) 100275

Contents lists available at ScienceDirect

Biofilm

journal homepage: www.sciencedirect.com/journal/biofilm

Nanowire arrays with programmable geometries as a highly effective anti-biofilm surface

Marina A. George [a,b,c], David McGiffin [d], Anton Y. Peleg [e,f], Roey Elnathan [a,b,g,h,*], David M. Kaye [i], Yue Qu [e,f,**], Nicolas H. Voelcker [a,b,g,***]

[a] Melbourne Centre for Nanofabrication, Victorian Node of the Australian National Fabrication Facility, Clayton, 3168, Australia
[b] Department of Materials Science and Engineering, Monash University, Clayton, 3168, Australia
[c] Department of Photochemistry and Photobiology, National Institute of Laser Enhanced Sciences, Cairo University, Giza, 12613, Egypt
[d] Department of Cardiothoracic Surgery, The Alfred and Monash University, Melbourne, 3004, Australia
[e] Infection Program, Monash Biomedicine Discovery Institute, Department of Microbiology, Monash University, Clayton, 3800, Australia
[f] Department of Infectious Diseases, The Alfred Hospital and School of Translational Medicine, Monash University, Melbourne, 3004, Australia
[g] Monash Institute of Pharmaceutical Sciences, Monash University, Parkville, 3052, Australia
[h] School of Medicine, Faculty of Health, Deakin University, Waurn Ponds, 3216, Australia
[i] Department of Cardiology, The Alfred Hospital and Monash Alfred Baker Centre for Cardiovascular Research, Monash University, Melbourne, 3004, Australia

ARTICLE INFO

Keywords:
Nanowires
Surface patterning
Programmable geometries
Anti-infective surfaces
Biofilms
And device-related infections

ABSTRACT

Biofilm-related microbial infections are the Achilles' heel of many implantable medical devices. Surface patterning with nanostructures in the form of vertically aligned silicon (Si) nanowires (VA-SiNWs) holds promise to prevent these often "incurable" infections. In this study, we fabricated arrays of highly ordered SiNWs varying in three geometric parameters, including height, pitch size, and tip diameter (sharpness). Anti-infective efficacies of fabricated SiNW arrays were assessed against representative laboratory reference bacterial strains, *Staphylococcus aureus* ATCC 25923 and *Escherichia coli* ATCC 25922, using a modified microwell biofilm assay representing microorganism-implant interactions at a liquid-solid interface. To further understand the role of individual geometric parameters to the SiNW-induced bacterial killing, SiNW arrays with stepwise changes in individual geometric parameters were compared. The force that NWs applied on bacterial cells was mathematically calculated. Our results suggested that NWs with specific geometries were able to kill adherent bacterial cells and prevent further biofilm formation on biomaterial surfaces. Tip diameter and pitch size appeared to be key factors of nanowires predetermining their anti-infectiveness. Mechanistic investigation found that tip diameter and pitch size co-determined the pressure that NWs put on the cell envelope. The most effective anti-infective NWs fabricated in our study (50 nm in tip diameter and 400 nm in pitch size for *S. aureus* and 50 nm in tip diameter and 800 nm in pitch size for *E. coli*) put pressures of approximately 2.79 Pa and 8.86 Pa to the cell envelop of *S. aureus* and *E. coli*, respectively, and induced cell lyses. In addition, these NWs retained their activities against clinical isolates of *S. aureus* and *E. coli* from patients with confirmed device-related infections and showed little toxicity against human fibroblast cells and red blood cells.

1. Introduction

The use of implantable medical devices such as central lines, urinary catheters, ventricular assist devices, and pacemakers is often complicated by the high incidence of device-related infections [1]. Biofilm formation by bacterial pathogens on the device surface is the root cause of these infections and exacerbates the already severe antimicrobial resistance (AMR) issue in hospital settings [2]. It represents an important microbial survival strategy that is characterized by highly dense cell growth mode, the presence of symbolic extracellular polymeric

This article is part of a special issue entitled: APB2024 published in Biofilm.

* Corresponding author. Melbourne Centre for Nanofabrication, Victorian Node of the Australian National Fabrication Facility, Clayton, 3168, Australia
** Corresponding author. Infection Program, Monash Biomedicine Discovery Institute, Department of Microbiology, Monash University, Clayton, 3800, Australia
*** Corresponding author. Melbourne Centre for Nanofabrication, Victorian Node of the Australian National Fabrication Facility, Clayton, 3168, Australia
E-mail address: yue.qu@monash.edu (Y. Qu).

https://doi.org/10.1016/j.bioflm.2025.100275
Received 25 November 2024; Received in revised form 12 March 2025; Accepted 24 March 2025
Available online 24 March 2025

substances (EPS), repressed microbial metabolic activities and altered gene expression of embedded cells, and extremely high tolerance to antimicrobial agents and host immune responses [2,3]. As most device-related infections cannot be completely cured by conventional antibiotics, removing infected devices often remains the only but undesirable option, highlighting the importance of preventing biofilm formation when the risk of microbial contamination does exist.

Anti-infective surfaces are thus highly sought-after for implantable medical devices to prevent device-related infections [4]. One widely adopted approach is the surface modification to create an environment unfavourable for bacterial attachment and further growth [5]. Chemical modifications of the surface with silver nanoparticles [6], fluorine [7], quaternary-ammonium compounds [8], or antibiotics [9] have all shown promising *in vitro* or even *in vivo* anti-infective effects. Such a strategy, however, may carry an unappreciated risk of inducing AMR due to long-term exposure of microorganisms to surface-bound antimicrobials [10]. In addition, chemical modification of the surface may compromise biocompatibilities of implanted devices with host cells [11]. Physical approaches have been explored as an alternative to chemical modification to generate anti-infective surfaces. Inspired by wings of cicadas, dragonflies and gecko skin that naturally prevent microbial attachment and kill adhered microorganisms, mechano-bactericidal nanostructured topographies were developed [12–14]. Equipped with unique geometric features, nanostructured surfaces have showed effects against various microbial species [15]. Such nature-inspired nanostructures have also been successfully replicated on synthetic materials such as titanium orthopaedic implants and demonstrated outstanding anti-infective properties [16–19].

It has been proposed that the bactericidal effect of nature-inspired nanostructured surfaces was conferred by mechanical interactions between the unique nanostructures and microbial cells [19,20]. Bacterial cell membranes can be suspended on neighbouring nanostructures, causing membrane deformation, stretching and breakdown, and consequential cell death [19,20]. Moreover, the mechano-bactericidal effect induces microbial lysis in a relatively short period before a genetic evolution is triggered, posing little risk of promoting AMR [5]. In addition to deforming and stretching the microbial cell envelope, other mechanisms have also been proposed for the lethality of nanostructures, including electrostatic attraction, modulation of microbial signal transduction pathways, and increased oxidative stress within microbial cells [7,21,22]. Key determinants underlying the anti-infectiveness of these mechano-bactericidal topographies are yet to be determined [7,8]. Published studies implicated that the lethality of highly ordered nanostructures might be associated with geometric parameters of NWs such as height, sharpness and spacing [9,11,20]. Ivanova et al. (2020) recently reported an important effect of NW height on nanostructure-induced bacterial death, with the most effective nanoarrays killing 95 ± 5 % of adhered *Pseudomonas aeruginosa* cells and 83 ± 12 % of *Staphylococcus aureus* cells, converting into average 1.30 and 0.77 log reductions of the cell populations, respectively [20]. From a microbiological viewpoint, the performance of these nanoarrays may still be insufficient to "weaponize" a device surface against biofilm-producing microbial pathogens. The importance of individual geometric parameters needs to be studied in depth, in order to guide the fabrication of more effective anti-infective nanostructured surfaces for implantable medical devices.

Nanostructures, and in particular NWs create a bio-interface at spatial scales relevant to mammalian and bacterial cells [23–25]. Recent advances in nanofabrication technologies have enabled the development of high-aspect-ratio nanostructures with a diverse range of geometrical characteristics including shape, diameter, height, and density [26–28]. Others have reported the flexibility of manipulating the anti-infective efficacy of NWs simply by changing the densities of NWs and their surface roughness [29]. This study aimed to fabricate highly ordered VA-SiNW arrays on biomaterial surfaces that effectively prevent the formation of pathogenic biofilms, by programming three geometric parameters of the NWs, including tip diameter, height and pitch size. The importance of individual geometric parameters for the anti-infectiveness of NWs was also evaluated and a mechanistic investigation performed.

2. Results

2.1. Fabrication of VA-SiNWs with different geometric characteristics

Seven VA-SiNW arrays differing in three geometric parameters, including height, pitch size and tip diameters (sharpness) were fabricated for this study (Table 1). To evaluate the impact of individual geometric parameters on the anti-infectiveness of the SiNW array, we systematically altered one parameter at a time while keeping the other two constants. Key parameters were evaluated: heights (1.5 μm and 2 μm), pitch sizes (400 nm and 800 nm), and tip diameter (50 nm, 100 nm, and 400 nm). The fabricated SiNW arrays showed a highly ordered structure, with rigid nanoneedles projecting from the substrate and covering the entire surface (Fig. 1). In contrast, the black silicon prepared in our laboratory had NWs randomly distributed on the substrate and lacking fixed geometries.

2.2. Tailored SiNW arrays are highly effective in preventing biofilm growth on silicon substrates

We first validated biofilm growths of microorganisms in the custom-made microwell plate where bacterial cells could only interact with nanostructured surfaces. Upon overnight culture in the microwells, *S. aureus* cells grew as macrocolonies and microcolonies on the surface of flat silicon wafers (Fig. 2A), suggesting successful biofilm growths. Using the custom-made microwell plates, we then assessed SiNW arrays with different geometric characteristics for their anti-biofilm activities. Using PDMS as an untreated comparator, geometries 1, 2, and 5 were found to be effective in preventing biofilm formation by *S. aureus* ATCC 25923. Geometry 1 seemed to be more effective than all other tested SiNW arrays ($p = 0.001$), the flat silicon ($p = 0.006$), and the well-known anti-infective black silicon ($p = 0.001$) (Fig. 2B). Relative to untreated PDMS, SiNW geometry 1 reduced staphylococcal biofilm biomass by 3.25 ± 0.38 logs (mean ± SD) while the black silicon lowered biofilm growth by 1.61 ± 0.61 logs. For *E. coli* ATCC 25922, geometries 1, 2, 4, 5, 6 and 7 all effectively reduced biofilm formation, with geometry 7 outperforming all other SiNW arrays, the flat silicon, and the black silicon surfaces ($p < 0.05$). In our custom-made microwell plate, geometry 7 reduced biofilm formation of *E. coli* by 4.25 ± 0.79 logs and geometry 1 reduced biofilm growth by 2.54 ± 0.66 logs. Interestingly, black silicon did not show a significant anti-biofilm activity against *E. coli* in our testing system.

2.3. Sharpness and pitch size are key parameters for the anti-infectiveness of SiNW arrays

We further investigated the impact of individual geometric parameters on the anti-infectiveness of the SiNW arrays, by performing pairwise comparisons between different SiNW arrays. The sharpness appeared to play a key role in the anti-infectiveness of SiNW arrays. To

Table 1
VA-SiNW arrays with different geometric characteristics.

Geometries	Height	Pitch size	Tip diameter (sharpness)
1	2 μm	400 nm	50 nm
2	2 μm	400 nm	100 nm
3	2 μm	400 nm	400 nm
4	2 μm	800 nm	100 nm
5	1.5 μm	400 nm	100 nm
6	1.5 μm	800 nm	100 nm
7	2 μm	800 nm	50 nm

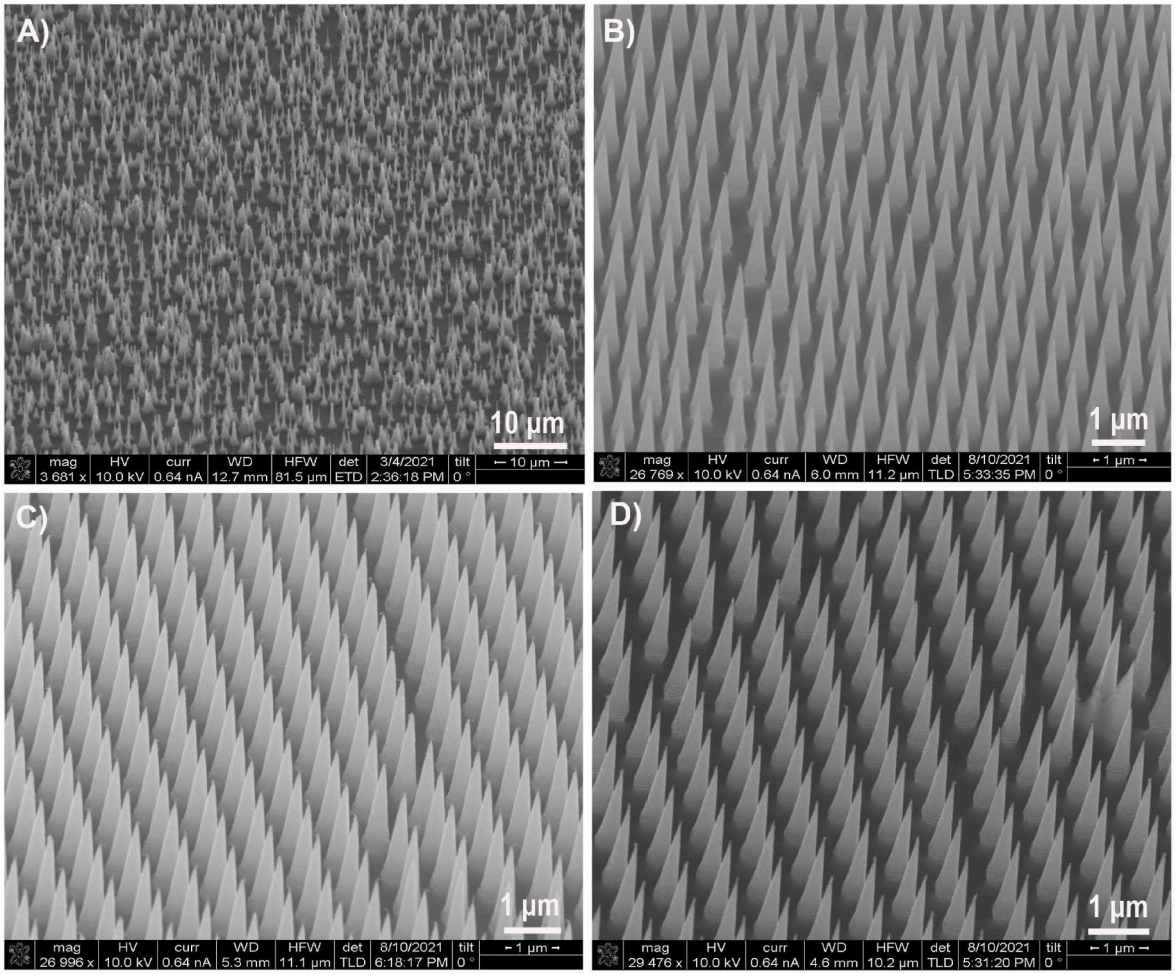

Fig. 1. A custom-made microwell plate. Nanostructured Si surfaces were placed between the top and bottom plates as the bottom of microwells. O-rings were used to avoid the leak of bacterial suspensions from microwells. Each microwell has a diameter of 8 mm and holds a volume of 250 μL. This microwell plate can be disassembled after incubation and individual nanosurfaces can be removed for detailed analyses.

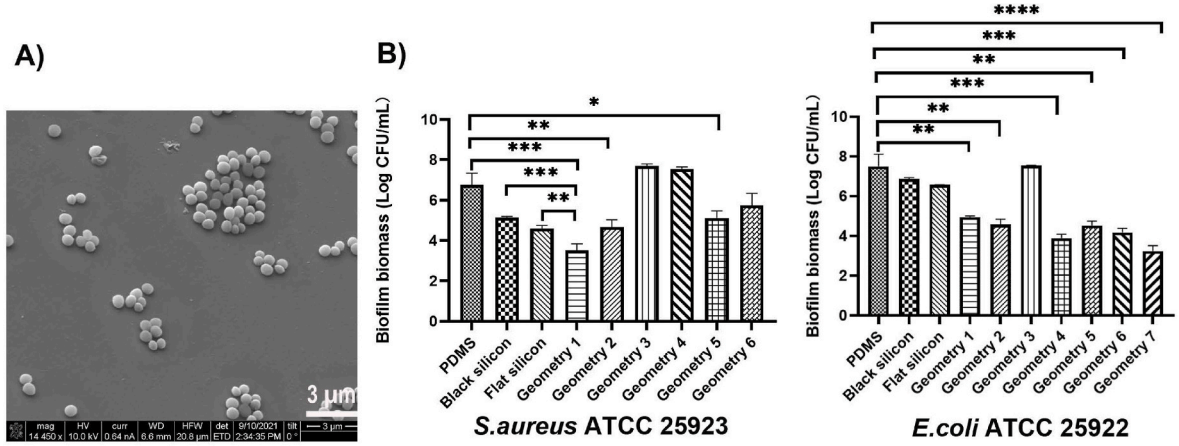

Fig. 2. Ultrastructure of fabricated SiNWs and black silicon. A) Black silicon, B) SiNW array of geometry 4, C) SiNW array of geometry 6, and D) SiNW array of geometry 7.

evaluate the link between the sharpness and bactericidal activity of SiNWs, we compared three geometries with same height and pitch size but different tip diameters for their anti-biofilm properties against *S. aureus* (Fig. 2B). Stepwise increases in biofilm formation by *S. aureus* ATCC 25923 were noticed for geometries 1, 2, and 3, in which the tip diameter was increased from 50 nm, 100 nm–400 nm. Further changing the pitch size from 400 nm to 800 nm (geometries 2 vs 4, 5 vs 6) led to a significant increase in biofilm formation of *S. aureus*, suggesting an additional role of pitch size in the anti-infectiveness of SiNWs.

Divergent results were obtained when Gram-negative bacterium

E. coli ATCC 25922 was tested. Evident anti-biofilm activities were found for SiNWs with a sharpness of 50 nm or 100 nm, but not for that with a sharpness of 400 nm (geometry 3, Fig. 2B). Increasing the pitch size from 400 nm to 800 nm (geometry 1 vs. geometry 7), however, significantly reduced *E. coli* biofilm formation by 1.71 ± 0.29 logs in the microwell biofilm assay ($p = 0.045$). Among all fabricated geometries, the SiNW array of geometry 7 showed the greatest anti-biofilm activity.

We also compared two pairs of geometries that only differed in SiNW heights (geometries 2 versus 5, and geometries 4 versus 6). Changing height from 1.5 μm to 2 μm did not show any impact on biofilm growth of *S. aureus* or *E. coli* on nanostructured surfaces ($p > 0.05$).

SiNWs exerted their anti-biofilm effects by inducing bacterial lyses.

SEM was carried out for qualitative analyses of microorganism-SiNW interactions (Fig. 3). In agreement with quantitative results, *S. aureus* formed biofilms more extensively on SiNW arrays with geometries 3 and 4 in comparison to geometry 1. A complete or partial lysis of most *S. aureus* cells in contact with NWs was seen on the SiNW surface of geometry 1 (Fig. 3A). Co-existence of intact staphylococcal cells, cells with rough surfaces, and cell debris were found for SiNW arrays of geometry 2 and 5 (Fig. 3A). Healthy-looking cells with smooth cell surface were found on the SiNW array of geometry 3 that has a sharpness of 400 nm or the SiNW array of geometry 6 with a pitch size of 800 nm (Fig. 3A). Robust biofilms were formed by *S. aureus* on untreated PDMS and few adherent monolayers were found on the negative control flat silicon after overnight culturing (Fig. 3A). In contrast, black silicon supported sporadic growth of microcolony biofilms (Fig. 3A). *E. coli* seemed to readily grow as adherent monolayers or biofilms on flat silicon (Fig. 3B). Presentation of SiNW arrays of geometries 2 and 7 to bacteria led to partial or complete lyses of bacterial cells (Fig. 3B).

A striking observation in our SEM study was that SiNW array of geometry 1 exerted physical force on the bottom of staphylococcal cells and induced the formation of "holes" on the contralateral surface of the cells (Fig. 3A, black arrow and Fig. 4A). To further confirm the observed phenotype was not due to an experimental artefact, we introduced the filter-disk based biofilm assay that only allows limited movement of bacterial cells on the nanostructured surface and would not permit cell turnover. Staphylococcal cells exposed to the SiNW array of geometry 1 in the filter disk-based biofilm assay showed different phases of membrane eruption in the opposite of where it was in contact with NWs, including cap formation (Fig. 4B), hole formation (Fig. 4C) and complete cell lysis (Fig. 4D).

2.4. Sharpness and pitch size co-determine the pressure applied by SiNWs on bacterial cell envelope

We noticed that SiNW arrays with a larger pitch size (800 nm vs 400 nm, with same height and sharpness) allowed fewer biofilm growths by *E. coli* (geometries 4 vs. 2, $p = 0.02$; geometries 7 vs 1, $p < 0.001$) but greater biofilm growth by *S. aureus* (geometry 4 vs. 2, $p < 0.001$). It is known that nanostructured surfaces kill bacterial cells by inducing deformation and penetration of the cell envelope, triggering oxidative stress [22] or membrane eruption [12]. *E. coli* and *S. aureus* differ physically in their morphology/size and cell wall structure. To understand the mechanistic bases of SiNW-induced bacterial killing, and more specially, how sharpness and pitch size of SiNWs co-determine their anti-infectiveness, we assessed the pressure placed by SiNWs with different geometries to the cell envelope of *S. aureus* and *E. coli*, which consequentially induced bacterial lyses.

According to SEM, adhered *S. aureus* cells had a diameter of 634 ± 59 nm, or an average volume of 1.34×10^{-19} m^3 (Table 2). For *E. coli*, the length and width of single cells were 1546 ± 368 nm and 456 ± 26 nm, respectively, and the average volume was 2.53×10^{19} m^3 (Table 2). Using the microbiological weight measurement method, a single cell of *S. aureus* weighed $2.37 \pm 0.25 \times 10^{-12}$ g and that for *E. coli* was $5.57 \pm 1.53 \times 10^{-12}$ g. The buoyancy force (FB) of a single cell in the MHB (biofilm growth medium) was then calculated using the formula FB = Vρg, where V is the volume of the cell, ρ is the density of MHB, and g is the gravitational acceleration. The FB for *S. aureus* ATCC25923 was calculated as 1.32 x 10 ^{15} N and for *E. coli* ATCC25992 was 2.49 x 10 ^{15} N.

We then calculated the pressure [(gravity force-buoyancy force)/area] that SiNWs placed on the cell envelope and ultimately triggered cell death. We used the area of cross section of the NW tip as the area of contact between the cell envelope and a single SiNW (A). The average number of SiNWs of different pitch sizes required to support a *S. aureus* or an *E. coli* cell (B) was obtained from high-resolution SEM images, by examining at least 10 cells. The total area of contact between a single cell and SiNWs equals (A x B).

Simplified calculations of the pressure placed by different SiNWs on a single bacterial cell in the modified microwell plate biofilm assay is presented in Table 2. Tip diameter and pitch size of NWs appear to co-determine the pressure applied by SiNWs on the bacterial cell envelope. The pressure that geometry 1 placed on the cell envelope of *S. aureus* ATCC 25923 was 2.79 Pa (see Table 2). Increasing the tip sharpness from 50 nm to 100 nm amplified the area of contact by four times and lowered the pressure to 0.70 Pa. Increasing the pitch size from 400 nm to 800 nm allowed staphylococcal cells to fall into gaps between NWs and consequentially survived on the surface. The pressure on *E. coli* ATCC 25922 by geometry 7 was 8.86 Pa. Lowering the pitch size from 800 nm to 400 nm (geometry 1) increased the number of NWs in contact with the *E. coli* cell envelop from 3 to 5, and consequentially reduced the pressure to 5.31 Pa.

2.5. SiNWs exhibit excellent anti-infective activities against clinical isolates causing device-associated infections

S. aureus SVH001, *S. aureus* SVH002, and *S. epidermidis* BioVAD15 from patients with confirmed VAD driveline infections [30], and a New Delhi metallo-β-lactamase *E. coli* from a patient with bloodstream infections at the Alfred Hospital, Melbourne were used to evaluate the anti-biofilm efficacies of SiNWs against clinical isolates. The three staphylococcal clinical isolates formed strong, intermediate, and weak biofilms on medical-grade silicone disks, supported by both colony-forming-unit (CFU) enumeration assay and confocal laser scanning microscopy (CLSM) (Fig. S1, see supplementary materials for the detailed method). The *E. coli* clinical isolate also demonstrated a substantial ability to form biofilms on the same biomaterial (Fig. S1). In agreement with what was found on laboratory reference strains, the top performing SiNW arrays (geometries 1 and 7) effectively prevented biofilm formation of all clinical isolates when grown for 24 h (Fig. 5A). Our SiNWs again outperformed black silicon when challenged by these clinical isolates; black silicon in some cases, failed to demonstrate better anti-infective activities than the positive control PDMS. We also noticed that the top-performing nanostructured surfaces did not show superiority over the flat silicon that is known to be resistant to short-term bacterial adherence [31] (Fig. 5A). Using *S. epidermidis* BioVAD15 as a representative, we extended biofilm growth in the microplate to 72 h. Upon long-term exposure, a large number of biofilms were formed on the flat silicon, reaching the amounts of biofilms formed on PDMS and black silicon (Fig. 5B). In contrast, geometry 1 retained an excellent anti-infectiveness and only allowed biofilm formation to a level similar to that of 24 h.

2.6. SiNWs demonstrated excellent biocompatibility towards human cells

All fabricated SiNWs showed negligible negative effects on human RBC, causing less than 1 % of hemolysis when using 2 % Triton X-100 as the positive control (Fig. 6A). There was no difference in biocompatibilities with RBCs between SiNWs and the original substrate flat silicon or medical grade PDMS. The NWs also showed little toxicity against human fibroblast cells (Fig. 6B), with 70–95 % of fibroblast cells surviving on different SiNWs, similar to that of PDMS.

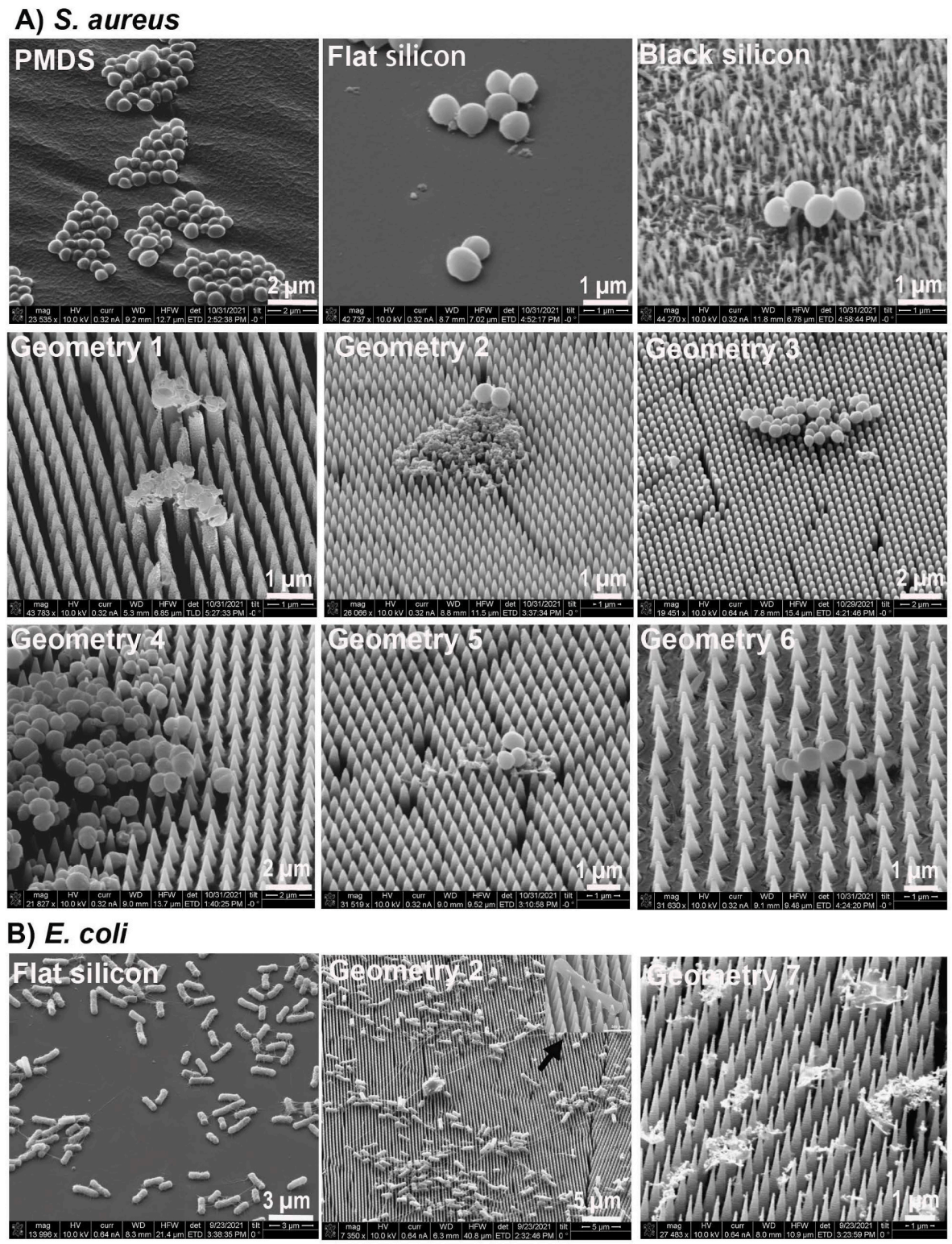

Fig. 3. Validation of the modified microwell biofilm assay and quantitative assessment of anti-biofilm efficacies of fabricated nanosurfaces. A) Scanning electron microscopy of *S. aureus* biofilms grown on flat silicon wafers. Biofilms were grown for 24 h at 37 °C with gentle shaking (75 rpm). **B)** Quantitative analyses (CFU enumeration) of biofilm formation by *S. aureus* and *E. coli* on SiNW arrays and control surfaces. The experiments were carried out in three biological repeats and error bars represent standard errors of the mean. * $0.01 < p \leq 0.05$, ** $0.001 < p \leq 0.01$, *** $0.0001 \leq P \leq 0.001$, **** $p < 0.0001$. SiNW surface of geometry 7 was not tested for *S. aureus* ATCC 25923 as our preliminary scanning electronic microscopy study found that staphylococcal cells fell into gaps between nanowires and no evident anti-biofilm efficacy was observed.

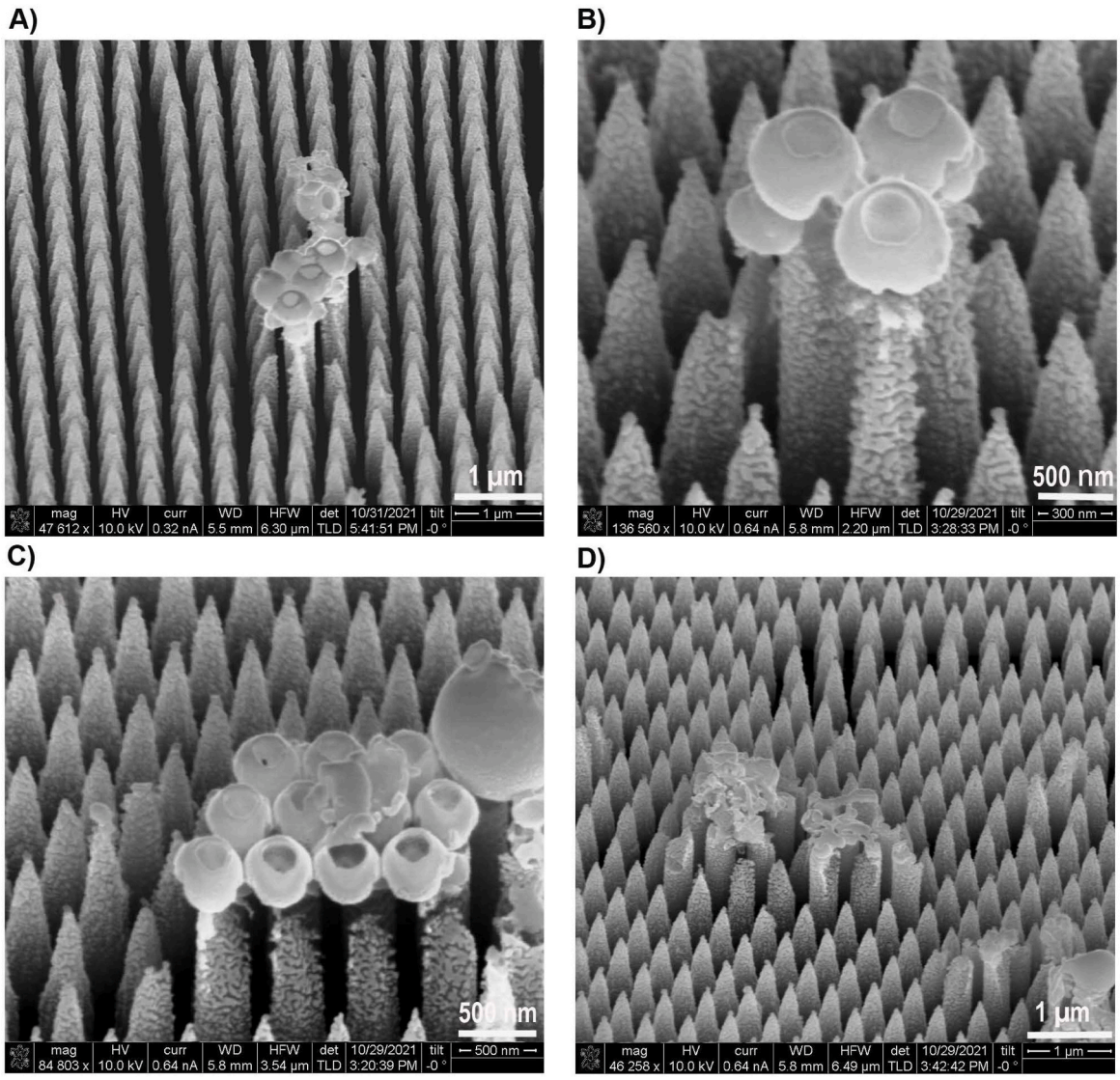

Fig. 4. Scanning electron microscopy (SEM) of *S. aureus* (A) and *E. coli* interacting with SiNWs (B). Bacterial cells at a density of ~1 × 10^7 CFU/mL (100 µL) were grown on SiNWs, using the custom-made microwell plates for cultivation and Muller-Hinton broth as the growth medium. The incubation was carried out at 37 °C for 24 h, with gentle shaking (75 rpm).

3. Discussion

Nanostructured surfaces hold the promise to prevent difficult-to-treat medical device infections. Processes used to fabricate synthetic nanostructured surfaces have often resulted in the inadvertent modification of various surface characteristics and therefore the importance of exact geometrical parameters of nanostructures on their antibacterial properties are not fully understood [26]. In the current study, we fabricated highly ordered SiNW arrays, with rigid nanoneedles projecting from the surface and forming a defensive layer.

These specifically designed SiNWs demonstrated outstanding anti-biofilm activities *in vitro*. Inspired by antibacterial cicada wings [12], Ivanova et al. (2013) fabricated the very first nanostructured bactericidal surfaces on synthetic materials [32]. The "black silicon" was prepared by reactive ion etching (RIE) on silicon substrates, imitating the wings of the dragonfly via the fabrication of nanoprotruding surfaces featuring NWs with high aspect ratios of 500 nm in length and 20–80 nm in tip diameter [32]. These black silicon NWs were often randomly distributed on surface, lacking fixed specific geometry of above-mentioned parameters. Our top performing SiNWs significantly outperformed black silicon in preventing biofilm growth by staphylococci and *E. coli*, including both laboratory reference strains and clinical isolates.

In a study by Ivanova et al., the bactericidal activity of black silicon has been explained by physical forces exerted by surface structures (or stresses generated by them) on bacterial cells and further induce cell deformation and lysis [32]. Several factors that may affect the bactericidal activity of black silicon have been proposed, including the overall magnitude, and more specifically, NW heights, tip diameters, and pitch sizes [32]. We carried out an experimental study to clarify the importance of individual geometries on the anti-infectiveness of nanostructured surfaces. By making stepwise changes of each parameter, we found the sharpness had the most important impact on the anti-biofilm activities of SiNWs, followed by the pitch size. It was noticed that a pitch size of 400 nm was needed for the most effective anti-biofilm activity against *S. aureus*, while a pitch size of 800 nm was preferred for *E. coli*. Gram-positive cocci and Gram-negative rods differ in cell size; changes in pitch size may lead to difference in the number of NWs required to hold up a single bacterial cell and consequentially different pressure placed by NWs on the cell envelope. The role of NW height seemed to be

Table 2
Pressure placed by SiNWs to the cell envelope to induce bacterial lyses.

Bacterial strains	*S. aureus* ATCC 25923			*E. coli* ATCC 25922		
Silicon nanowires (SiNWs)	Geometry 1 (most effective)	Geometry 2 (less effective)	Geometry 4 (ineffective)	Geometry 7 (most effective)	Geometry 1 (less effective)	Geometry 3 (ineffective)
Average weight of a single cell (mass)	2.37×10^{-12} g			5.57×10^{-12} g		
Gravity = mass · g (9.8 N/kg)	2.32×10^{-14} N			5.46×10^{-14} N		
ρ (density of MHB[c])	1002.2 g/L			1002.2 g/L		
Sizes/volume of a single cell	Diameter = 634.4 nm/1.34×10^{-19} m^3			Length = 1547 nm, width = 457 nm/2.54×10^{-19} m^3		
Buoyancy force = ρVg	1.32 x10 $^{-15}$ N			2.49 x10 $^{-15}$ N		
Net force (F)[b]	2.19×10^{-14} N			5.21×10^{-14} N		
Tip diameters	50 nm	100 nm	100 nm	50 nm	50 nm	400 nm
Contact area of a single nanowire and a cell[#]	1.96 x10 $^{-15}$ m^2	7.84 x10 $^{-15}$ m^2	7.84 x10 $^{-15}$ m^2	1.96 x10 $^{-15}$ m^2	1.96 x10 $^{-15}$ m^2	1.26 x10 $^{-13}$ m^2
Pitch sizes	400 nm	400 nm	800 nm	800 nm	400 nm	400 nm
No. of nanowires in contact with a cell	4	4	0 [a]	3	5	5
Total contact area (A)	7.84×10^{-15} m^2	3.13×10^{-14} m^2	0	5.88×10^{-15} m^2	9.80×10^{-15} m^2	6.30×10^{-13} m^2
Pressure (P)= F/A	**2.79 Pa**	**0.70 Pa**	**0 Pa**	**8.86 Pa**	**5.31 Pa**	**0.08 Pa**

r = 1/2 tip diameter.
[a] Most staphylococcal cells were found to fall into the gaps between nanowires; *Contact area of one nanowire and a cell was calculated as πr^2.
[b] Net force = Gravity force – buoyancy force.
[c] MHB, Muller-Hinton broth.

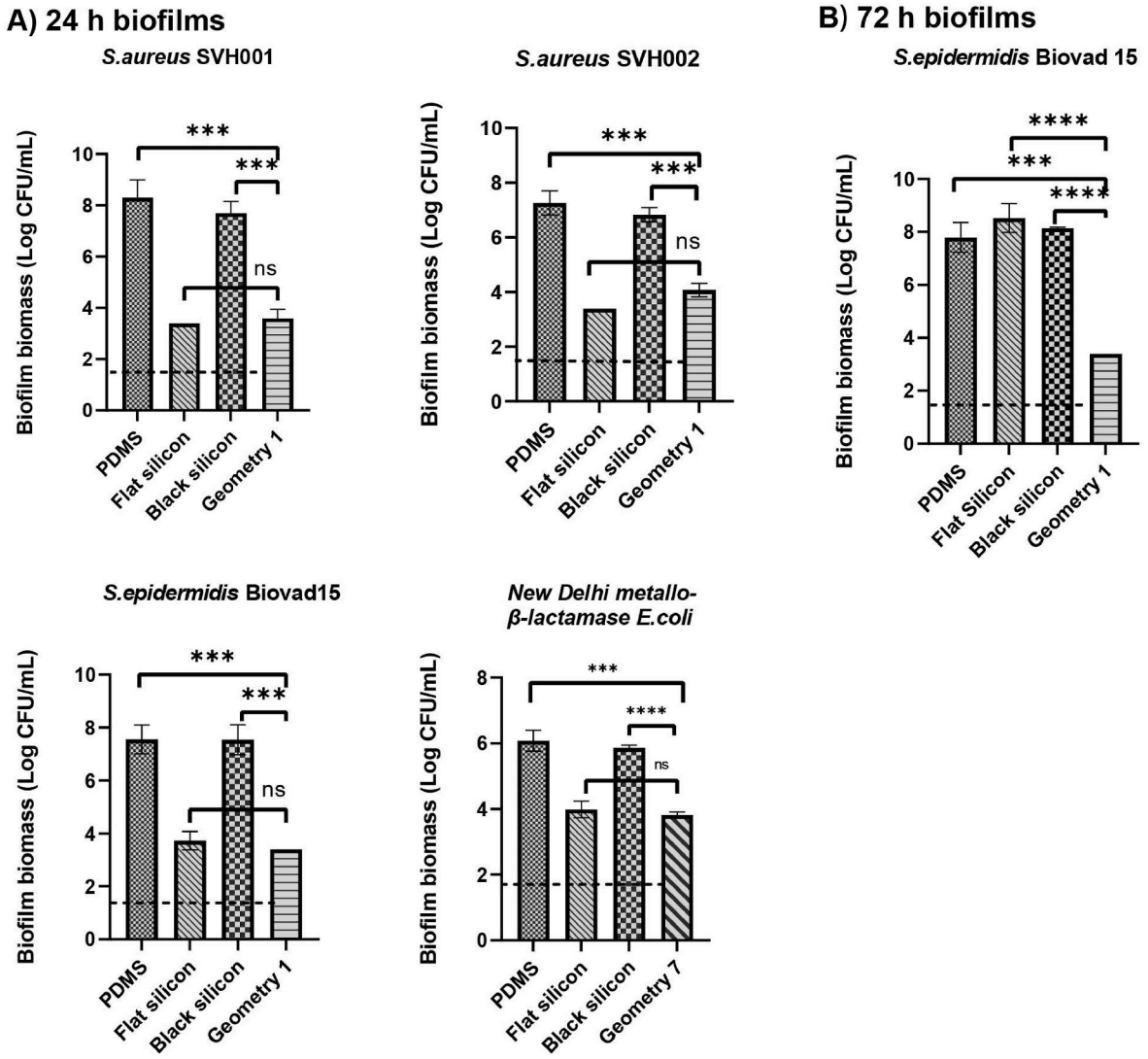

Fig. 5. SEM of *S. aureus* cells exposed to SiNW of geometry 1. A) Using the modified microwell plate biofilm assay, B-D) Using the filter-disk based biofilm assay.

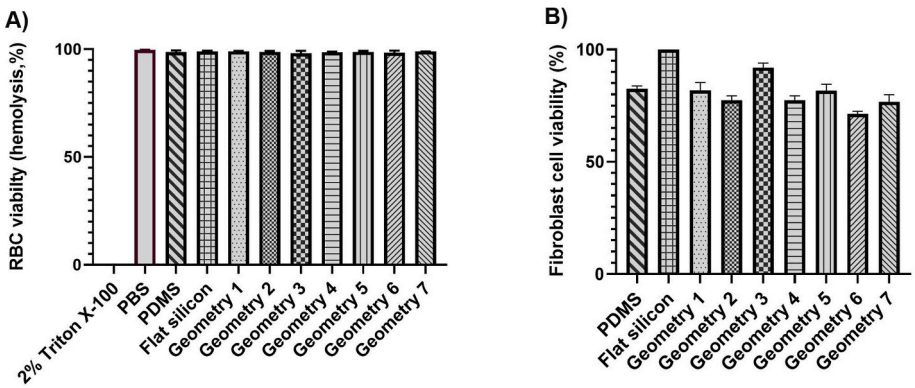

Fig. 6. Anti-infective efficacies of nanostructured surfaces against biofilm formation by clinical isolates. A) 24 h biofilm growths by clinical isolates on nanostructured and control surfaces. The most effective SiNWs were selected for this experiment. B) 72 h biofilm growths by *S. epidermidis* clinical isolate BioVAD15 on nanostructured and control surfaces. The experiments were carried out in three biological repeats and error bars represent standard errors of the mean. * $0.01 < p \leq 0.05$, ** $0.001 < p \leq 0.01$, *** $0.0001 \leq P \leq 0.001$, **** $p < 0.0001$. Dashed lines, detection limit.

paradoxical between our study and that by Ivanova et al. (2020) [20]; it is possibly that the impact of NW height on their antibacterial activities reported by Ivanova et al. was due to tilting of the NW with greater height and reduction of contact area at the NW-cell interface [20,32].

With focused ion beam (FIB)-SEM, others have showed that NWs pressed the cell envelope, stretching the local membrane of bacterial cells and ultimately leading to cell death [32]. Using mathematical modelling, our study further revealed that the sharpness and pitch size combinationally determined the pressure placed by SiNWs on the cell envelope; SiNWs with the most effective geometries placed a pressure of 2.79 Pa on *S. aureus* or 8.86 Pa on *E. coli*, respectively, and induced cell lyses. It was evident that doubling the sharpness reduced the pressure on the bacterial envelope by four times, supporting that notion that the sharpness is a key regulator for the anti-infective efficacy of SiNWs. Pitch size influences bactericidal activities of nanostructures at a smaller magnitude.

A striking observation of this study is the anti-infective NWs induced eruption or formation of "holes" on the cell membranes of *S. aureus* opposite to where the NWs were in contact with bacterial cells. We hypothesised that the pressure placed by SiNWs on the *S. aureus* cell envelop may have activated over-expression of *alt* and autolysin-associated molecular pathways [33]. A future study should be carried out to clarify the molecular mechanisms underlying the nanostructure-induced bacterial cell lysis.

We also assessed the translational potential of SiNWs for clinical application. The SiNWs retained activities against biofilms formed by multidrug-resistant clinical isolates of *S. aureus*, *S. epidermidis* and *E. coli*, and showed excellent biocompatibilities with both human RBCs and fibroblast cells. The biocompatibilities of SiNWS were similar to that of PDMS, which is widely used for implantable medical devices such as VAD drivelines and central venous catheters. The other important characteristics that are vital for successful clinical translation include the stability and hydrophobicity of NWs. The stability of the NWs post-DRIE is dependent on their aspect ratio and the etching parameters. High aspect ratio NWs might be mechanically fragile. The conical-shaped NWs fabricated in our study have a wide base, and thus are not prone to bending or breaking. The stability of the NW surfaces was supported by SEM images showing the integrity of NW ultrastructure was not compromised after overnight repression by the saturated filter disk (Fig. 4). Surface hydrophilicity or hydrophobicity is another important characteristic that may affect the *in vivo* anti-infective effectiveness of NWs. After a medical device is implanted *in vivo*, its surface will be immediately coated by host matrix proteins and lipids that may facilitate bacterial adherence and biofilm formation. A highly hydrophilic surface often resists nonspecific protein or eDNA adsorption and is preferred for implantable medical devices [34]. Although NW surface are typically hydrophobic post-DRIE treatments, further surface functionalization is able to tune the hydrophobicity and hydrophilicity of the NW surface, depending on the selection of ligand for functionalization [34].

We acknowledge that this study still suffers from limitations. This proof-of-concept study only used two laboratory reference strains and four clinical isolates. The anti-infective activities of SiNWs fabricated here may not be appliable for biofilms formed by other microbial species or strains. Nanostructure-mediated physical killing effects depend on the contact of bacterial cells with the substrate. In this study, we placed the nanostructured surface in the bottom of the testing systems to allow the gravity to act as the major force to push cells towards the fabricated surface. The importance of geometric parameters of nanostructures on their anti-infectiveness needs to be further studied for more complicated infection microenvironments, such as biofilms formed on the wall of a three-dimensional medical device or in a dynamic cultivation system. A flow culture condition is more relevant to practical scenarios than static conditions, such as catheter-related bloodstream infections and urinary tract infections, where bacterial attachment often occurs under shear forces. Also, we cannot deny the *in vitro* nature of this study. The anti-infective efficacy and biosafety of fabricated SiNWs should be further assessed using small animal models such as subcutaneous implant biofilm model and percutaneous implant model to advance the application of this nanostructured weapon to a pre-clinical phase.

4. Conclusion

In conclusion, we fabricated patterned anti-infective nanostructured surfaces featuring highly ordered SiNWs with tailored geometrical parameters including height, pitch size and tip diameter, and further evaluated their efficacies in preventing biofilm formation by common bacterial pathogens. Mechanistically, individual geometrical parameters impacted the anti-infectiveness of SiNWs by influencing the amount of pressure placed by the nanostructure on the bacterial cell envelope. Our findings underscore the importance of taking into consideration of two key geometrical parameters of NWs, tip diameter and pitch size when designing nanostructures for anti-infective purposes.

5. Experimental sections

5.1. Fabrication of SiNWs

Flat silicon (Si) wafers (3″, p-type, 3–6 Ω cm,⟨100⟩, Siltronix, France) were cut into four pieces, sonicated in a mixed solution of ethanol and acetone (ratio 1:1) for 10 min, and washed with distilled water for 10 min. Si was selected for its surface tailorability, and biocompatibility

[20,35,36]. To remove any organic contaminants, Si wafers were dipped into boiling Piranha solution (3:1H_2SO_4:H_2O_2 v/v, 75 °C) for 1 h followed by washing with distilled water and blow drying with N_2 gas.

Convective assembly deposition: Hexagonally close-packed monolayer of polystyrene microsphere (1 μm, PSMS, Polysciences, Inc.) were deposited over a Si wafer by convective assembly [37,38]. Convective assembly is a technique where microscope slide is mounted and used as a blade marker for the PSMS depositions. 25 μL of PSMS suspension (2.5 % w/v in water) was placed on the slide and a 50 mm motorised translation stage (MTS50-Z8, Thorlabs, Inc.) was used to deposit a uniform monolayer of PSMS.

Oxygen plasma treatment of PSMS: Samples were inserted into Plasmalab100 ICP380 deep reactive ion etcher (Oxford Instruments), where oxygen plasma treatment was performed in order to reduce the size of the PSMS. A flow rate of 100 SCCM O_2 was used with inductively coupled plasma (ICP) power of 100 W and bias power of 50 W. PSMS served as a mask for the subsequent Si etching in two steps.

Deep reactive ion etching (DRIE): The DRIE technique was used to control every single parameter independent from others, fabricating consistent nanostructures and constructing large scale of highly ordered NWs [39,40]. This consisted of two consecutive steps; 1) Bosch process: Si etching was performed by alternate cycles of passivation and etching steps to obtain VA-SiNW. During the passivation step (8 s), a flow rate of 100 sccm C_4F_8 and 10 sccm SF_6 was used with ICP power of 1000 W and bias power of 5 W. During the etching step (6 s), a flow rate of 100 sccm SF_6 and 10 sccm C_4F_8 was used with ICP power of 1000 W and bias power of 20 W. The depth of etching (height of VA-SiNW) was controlled by the number of cycles. This was followed by removing PSMS by sonication of Si wafers in distilled water for 2 min. Samples were then dried under N_2 gas and inserted back to the DRIE for the next step. 2) Pseudo-Bosch process: To achieve a tapered VA-SiNW profile, etching was performed with a simultaneous flow of 100 sccm SF_6 and 40 sccm C_4F_8 at a pressure of 10 mTorr, with ICP power of 1000 W and bias power of 50 W. The tip diameter and the final height of the VA-SiNW were controlled by etching time. Untreated flat silicon was used as a negative control and black silicon was introduced as a benchmark control due to its well-known anti-infective performance. Black silicon was fabricated as described by Ivanova et al. (2013) [32].

5.2. Microorganisms

Two laboratory reference strains were selected for this study, *S. aureus* ATCC 25923 and *Escherichia coli* ATCC 25922 representing Gram-positive bacteria and Gram-negative bacteria respectively. A panel of clinical strains were also used in this study, including *S. aureus* SVH001, *S. aureus* SVH002, and *Staphylococcus epidermidis* BioVAD15 that were isolated from patients with confirmed ventricular assist device (VAD) driveline infections [30], and a multi-drug resistant New Delhi metallo-β-lactamase-positive *E. coli* from the Alfred Hospital, Melbourne, Australia.

5.3. Biofilm cultivation models

A modified microwell biofilm assay: Microplate-based biofilm assay has been widely used to study bacterial adherence to abiotic surfaces at a liquid-solid interface, such as those encountered in catheter-related bloodstream infections [41]. Directly placing NW-coated Si substrate into microwells, however, may yield erroneous results due to the exposure of untreated back and edge surfaces of the substrate to microorganisms. To address this issue, a novel microplate using fabricated nanosurfaces as the bottom was engineered (Fig. 7). This modified microwell plate allowed direct examination of interactions between NWs and bacterial cells at a liquid-solid interface.

Filter disc-based biofilm assay: A filter disc-based biofilm assay was adapted from a previously published work with modification to study bacterium-NW interactions at a solid-liquid-air interface (see Fig. 8) [42]. The specific microenvironment of this assay mimics that encountered in other biofilm-related infections such as ventricular assist device driveline exit-site infections or chronic wound infections and limits free movement of bacterial cells at the reversible attachment phase of biofilm formation [43].

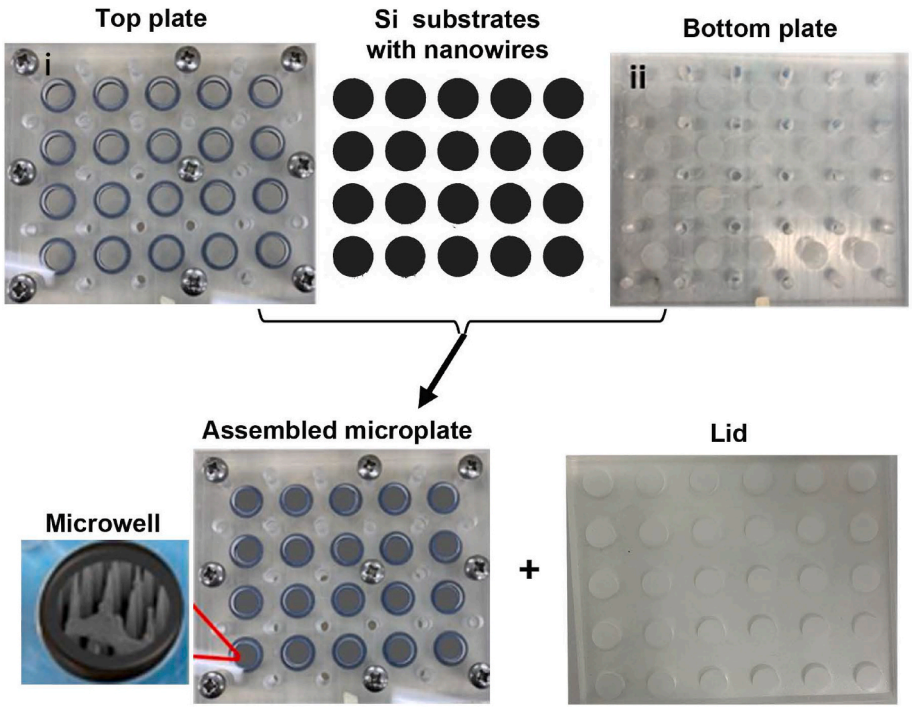

Fig. 7. Biocompatibilities of SiNWs. Human RBCs and fetal lung fibroblasts MRC5 were exposed to SiNWs and control surfaces for 2 h. RBC haemolysis (A) and MRC5 cell viability (B) were assessed respectively. These experiments were carried out in three biological repeats and error bars represent standard errors of the mean.

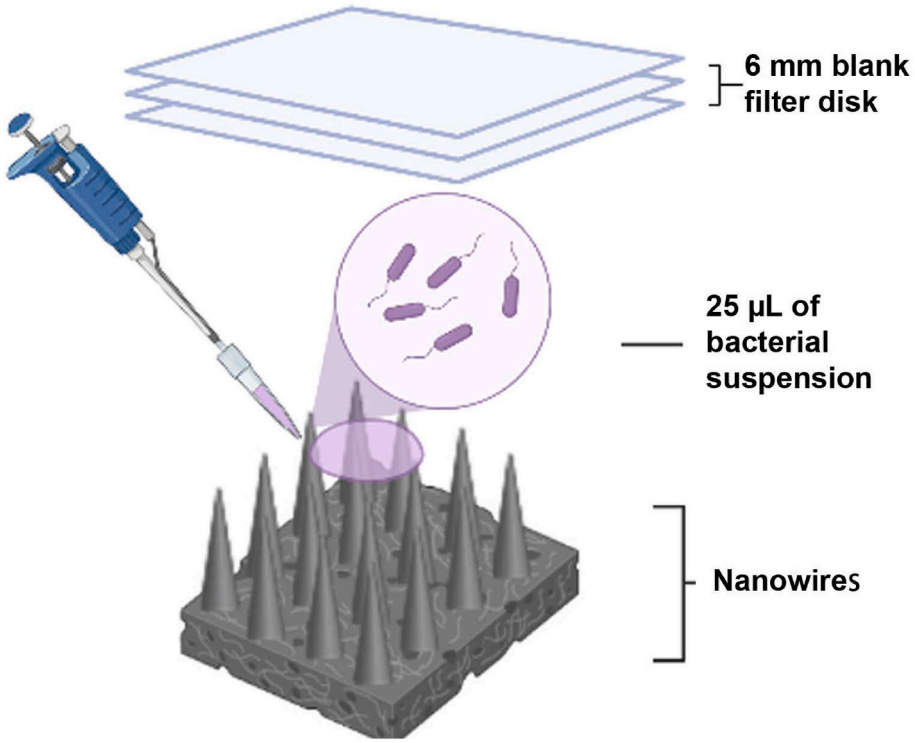

Fig. 8. Schematic description of the filter disc-based biofilm assay. The method was modified from a previously published method [42]. The set-up was incubated in a 37 °C humid chamber for 24 h. The growth medium (Muller-Hinton broth) was absorbed by the filter disk and bacterial cells were physically trapped between the nanowires and filter disks with very limited movement.

5.4. Quantitative and qualitative analyses of bacterial adherence and biofilm formation

Microbial biofilms were grown in the custom-made microwell plates, using Muller-Hinton broth (MHB, Oxoid, UK) as the growth medium and under gentle shaking (75 rpm), following a previously published method [41]. Viable cell enumeration was used to quantitatively evaluate bacterial adherence and biofilm growths on nanostructured surfaces. After disassembly, nanostructured samples were washed three times with phosphate buffered saline (PBS) before being transferred to Eppendorf tubes containing 1 mL of PBS, followed by vigorous vortex (30" x 4 times) and sonication (42 kHz × 10 min). Vortex and sonication allow preformed biofilms or adherent monolayers to detach from biomaterial surfaces and disassociate cell clusters into single cells. The biofilm cell suspensions were then serially diluted and 20 µL from each dilution were plated on nutrient agar plates for viable counts after overnight incubation at 37 °C. The viable biofilm cells are presented in the form of CFU per 1 mL of PBS.

Scanning electron microscopy (SEM) was used to qualitatively assess bacterial adherence and biofilm formation on nanostructured surfaces, as previously described [44]. Nanostructured samples were rinsed and washed with 0.1 M sodium cacodylate buffer (Electron Microscopy Sciences) and fixed with 2.5 % glutaraldehyde (Electron Microscopy Sciences) at 4 °C overnight. Samples were then washed gently (3 × 5 min) with chilled 0.1 m sodium cacodylate buffer and post fixed with 1 % osmium for 1 h. The fixed samples were gradually dehydrated with increasing concentrations of ethanol (50 %, 70 %, 90 %, and 100 %, 10 min each) at room temperature and critical point dried (CPD 030 Critical Point Dryer, BAL-TEC). Dehydrated samples were then sputter-coated with a 20 nm layer of gold to increase their conductivity for SEM imaging.

5.5. Weight measurement of single bacterial cells

The weight of single bacterial cells was measured using a published method with modification [45]. In brief, bacterial cells were grown in 25 mL of MHB to an early stationary phase (12–16 h). The total bacterial cell number in the suspension was determined using the viable cell enumeration method. The bacterial suspensions were centrifuged at 5500 rpm for 10 min and the cell pellets were fixed with 2.5 % glutaraldehyde to stop further cell growths and resuspended in 25 mL of PBS. Mixed cellulose ester (MCE) membrane filters (0.22 µm in pore-size, 47 mm in diameter) were used to remove the supernatants and collect the bacterial cells. The membrane with bacterial cells was then air-dried at 37 °C overnight. The weight of the cell population = dry weight of membrane after filtration – dry weight of the membrane before filtration. The weight of a single bacterial cell was calculated as weight of the cell population/number of single cells in the population.

5.6. Biocompatibility evaluation

Red blood cell (RBC) cytotoxicity test: Biocompatibility of nanostructured surfaces with human red blood cells was assessed using a published method with modifications [46]. A microwell plate with different SiNW-coated surfaces was prepared as described before. Human red blood cells were collected and washed three times with PBS. 0.5×10^5 RBCs prepared in 100 µL of PBS were added into each microwell; these RBCs were able to form a confluent monolayer on the NW surface in the microwell. 2 % Triton X-100 was used as a positive control and PBS served as a negative control. The set-up was incubated statically at 37 °C for 2 h. 80 µL of the supernatant was transferred to a 96-well microplate and haemolysis was examined by reading OD_{492}.

Fibroblast cytotoxicity test: Human fetal lung fibroblasts (MRC5, 20000 cells per well) were seeded on the NW-coated surface in the microwell plate and incubated in a CO_2 incubator for 2 h to allow the formation of a monolayer. The viability of MRC5 in the monolayer was

measured using the ATP-based CellTiter Glo kit (Promega, Madison, USA), following the manufacturer's instruction.

5.7. Statistical analysis

To analyse differences in microbial adherence, biofilm formation or biocompatibilities of different nanostructured surfaces, one-way ANOVA test or a non-parametric Mann-Whitney test was performed with Minitab Statistical Software 16 for Windows (Minitab Ltd., Coventry, UK) using a significance level of 0.05, depending on the data distribution.

CRediT authorship contribution statement

Marina A. George: Writing – original draft, Methodology, Investigation, Formal analysis, Data curation. **David McGiffin:** Writing – review & editing, Validation, Methodology, Funding acquisition, Formal analysis, Data curation. **Anton Y. Peleg:** Formal analysis, Data curation. **Roey Elnathan:** Writing – review & editing, Supervision, Resources, Methodology, Formal analysis. **David M. Kaye:** Writing – review & editing, Resources, Formal analysis, Data curation. **Yue Qu:** Writing – review & editing, Writing – original draft, Validation, Supervision, Methodology, Investigation, Funding acquisition, Formal analysis, Data curation, Conceptualization. **Nicolas H. Voelcker:** Writing – review & editing, Supervision, Funding acquisition, Formal analysis, Data curation, Conceptualization.

Ethics approval and consent to participate

Not applicable.

Consent for publication

Not applicable.

Availability of data and material

All data generated or analyzed during this study are included in this published article [and its supplementary information files].

Funding sources

Publication of this article was supported by the Medical Research Future Fund Artificial Heart Frontier Program (DM, DK, YQ, and AYP). This work was performed in part at the Melbourne Centre for Nanofabrication (MCN) in the Victorian Node of the Australian National Fabrication Facility (ANFF). R.E. wants to thank the Australian government, for his ARC Future Fellowship (project number: FT220100749).

Declaration of competing interest

The authors declare that they have no known competing financial interests or personal relationships that could have appeared to influence the work reported in this paper.

Appendix A. Supplementary data

Supplementary data to this article can be found online at https://doi.org/10.1016/j.bioflm.2025.100275.

Data availability

Data will be made available on request.

References

[1] VanEpps JS, Younger JG. Implantable device-related infection. Shock 2016;46(6):597–608. https://doi.org/10.1097/shk.0000000000000692. From NLM.
[2] Arciola CR, Campoccia D, Montanaro L. Implant infections: adhesion, biofilm formation and immune evasion. Nat Rev Microbiol 2018;16(7):397–409. https://doi.org/10.1038/s41579-018-0019-y. From NLM.
[3] Yang S, Hay ID, Cameron DR, Speir M, Cui B, Su F, Peleg AY, Lithgow T, Deighton MA, Qu Y. Antibiotic regimen based on population analysis of residing persister cells eradicates *Staphylococcus epidermidis* biofilms. Sci Rep 2015;5(1):18578. https://doi.org/10.1038/srep18578.
[4] Li W, Thian ES, Wang M, Wang Z, Ren L. Surface design for antibacterial materials: from fundamentals to advanced strategies. Adv Sci 2021;8(19):e2100368. https://doi.org/10.1002/advs.202100368. From NLM.
[5] Wang Y, Subbiahdoss G, Swartjes J, van der Mei HC, Busscher HJ, Libera M. Length-scale mediated differential adhesion of mammalian cells and microbes. Adv Funct Mater 2011;21(20):3916–23. https://doi.org/10.1002/adfm.201100659.
[6] Gosheger G, Hardes J, Ahrens H, Streitburger A, Buerger H, Erren M, Gunsel A, Kemper FH, Winkelmann W, Von Eiff C. Silver-coated megaendoprostheses in a rabbit model–an analysis of the infection rate and toxicological side effects. Biomaterials 2004;25(24):5547–56. https://doi.org/10.1016/j.biomaterials.2004.01.008. From NLM.
[7] Lepoittevin B, Bedel S, Dragoé D, Bruzaud J, Barthés-Labrousse M-G, Mazerat S, Herry J-M, Bellon-Fontaine M-N, Roger P. Antibacterial surfaces obtained through dopamine and fluorination functionalizations. Prog Org Coating 2015;82:17–25. https://doi.org/10.1016/j.porgcoat.2015.01.007.
[8] Asri LATW, Crismaru M, Roest S, Chen Y, Ivashenko O, Rudolf P, Tiller JC, van der Mei HC, Loontjens TJA, Busscher HJ. A shape-adaptive, antibacterial-coating of immobilized quaternary-ammonium compounds tethered on hyperbranched polyurea and its mechanism of action. Adv Funct Mater 2014;24(3):346–55. https://doi.org/10.1002/adfm.201301686.
[9] Cloutier M, Mantovani D, Rosei F. Antibacterial coatings: challenges, perspectives, and opportunities. Trends Biotechnol 2015;33(11):637–52. https://doi.org/10.1016/j.tibtech.2015.09.002. From NLM.
[10] Pietsch F, O'Neill AJ, Ivask A, Jenssen H, Inkinen J, Kahru A, Ahonen M, Schreiber F. Selection of resistance by antimicrobial coatings in the healthcare setting. J Hosp Infect 2020;106(1):115–25. https://doi.org/10.1016/j.jhin.2020.06.006.
[11] Ista LK, Pérez-Luna VH, López GP. Surface-grafted, environmentally sensitive polymers for biofilm release. Appl Environ Microbiol 1999;65(4):1603–9. https://doi.org/10.1128/aem.65.4.1603-1609.1999. From NLM.
[12] Ivanova EP, Hasan J, Webb HK, Truong VK, Watson GS, Watson JA, Baulin VA, Pogodin S, Wang JY, Tobin MJ, et al. Natural bactericidal surfaces: mechanical rupture of *Pseudomonas aeruginosa* cells by cicada wings. Small 2012;8(16):2489–94. https://doi.org/10.1002/smll.20120052. From NLM.
[13] Watson GS, Green DW, Schwarzkopf L, Li X, Cribb BW, Myhra S, Watson JA. A gecko skin micro/nano structure - a low adhesion, superhydrophobic, anti-wetting, self-cleaning, biocompatible, antibacterial surface. Acta Biomater 2015;21:109–22. https://doi.org/10.1016/j.actbio.2015.03.007. From NLM.
[14] Bhadra CM, Truong VK, Pham VT, Al Kobaisi M, Seniutinas G, Wang JY, Juodkazis S, Crawford RJ, Ivanova EP. Antibacterial titanium nano-patterned arrays inspired by dragonfly wings. Sci Rep 2015;5:16817. https://doi.org/10.1038/srep16817. From NLM.
[15] Tripathy A, Sen P, Su B, Briscoe WH. Natural and bioinspired nanostructured bactericidal surfaces. Adv Colloid Interface Sci 2017;248:85–104. https://doi.org/10.1016/j.cis.2017.07.030. From NLM.
[16] Green DW, Lee KK-H, Watson JA, Kim H-Y, Yoon K-S, Kim E-J, Lee J-M, Watson GS, Jung H-S. High quality bioreplication of intricate nanostructures from a fragile gecko skin surface with bactericidal properties. Sci Rep 2017;7(1):41023. https://doi.org/10.1038/srep41023.
[17] Dickson MN, Liang EI, Rodriguez LA, Vollereaux N, Yee AF. Nanopatterned polymer surfaces with bactericidal properties. Biointerphases 2015;10(2):021010. https://doi.org/10.1116/1.4922157. PubMed.
[18] Jäger M, Jennissen HP, Dittrich F, Fischer A, Köhling HL. Antimicrobial and osseointegration properties of nanostructured titanium orthopaedic implants. Materials 2017;10(11). https://doi.org/10.3390/ma10111302. From NLM.
[19] Modaresifar K, Azizian S, Ganjian M, Fratila-Apachitei LE, Zadpoor AA. Bactericidal effects of nanopatterns: a systematic review. Acta Biomater 2019;83:29–36. https://doi.org/10.1016/j.actbio.2018.09.059. From NLM.
[20] Ivanova EP, Linklater DP, Werner M, Baulin VA, Xu X, Vrancken N, Rubanov S, Hanssen E, Wandiyanto J, Truong VK, et al. The multi-faceted mechano-bactericidal mechanism of nanostructured surfaces. Proc. Natl. Acad. Sci. U.S.A 2020;117(23):12598–605. https://doi.org/10.1073/pnas.1916680117. From NLM.
[21] Darouiche RO. Treatment of infections associated with surgical implants. N Engl J Med 2004;350(14):1422–9. https://doi.org/10.1056/NEJMra035415. From NLM.
[22] Jenkins J, Mantell J, Neal C, Gholinia A, Verkade P, Nobbs AH, Su B. Antibacterial effects of nanopillar surfaces are mediated by cell impedance, penetration and induction of oxidative stress. Nat Commun 2020;11(1):1626. https://doi.org/10.1038/s41467-020-15471-x. From NLM.
[23] Chen Y, Wang J, Li X, Hu N, Voelcker NH, Xie X, Elnathan R. Emerging roles of 1D vertical nanostructures in orchestrating immune cell functions. Adv Mater 2020;32(40):e2001668. https://doi.org/10.1002/adma.202001668. From NLM.
[24] Shokouhi AR, Chen Y, Yoh HZ, Brenker J, Alan T, Murayama T, Suu K, Morikawa Y, Voelcker NH, Elnathan R. Engineering efficient CAR-T cells via

electroactive nanoinjection. Adv Mater 2023;35(44):e2304122. https://doi.org/10.1002/adma.202304122. From NLM.
[25] Chen Y, Mach M, Shokouhi A-R, Yoh HZ, Bishop DC, Murayama T, Suu K, Morikawa Y, Barry SC, Micklethwaite K, et al. Efficient non-viral CAR-T cell generation via silicon-nanotube-mediated transfection. Mater Today 2023;63:8–17. https://doi.org/10.1016/j.mattod.2023.02.009.
[26] Chiappini C, Chen Y, Aslanoglou S, Mariano A, Mollo V, Mu H, De Rosa E, He G, Tasciotti E, Xie X, et al. Tutorial: using nanoneedles for intracellular delivery. Nat Protoc 2021;16(10):4539–63. https://doi.org/10.1038/s41596-021-00600-7. From NLM.
[27] Elnathan R, Barbato MG, Guo X, Mariano A, Wang Z, Santoro F, Shi P, Voelcker NH, Xie X, Young JL, et al. Biointerface design for vertical nanoprobes. Nat Rev Mater 2022;7(12):953–73. https://doi.org/10.1038/s41578-022-00464-7.
[28] Chen Y, Shokouhi A-R, Voelcker NH, Elnathan R. Nanoinjection: a platform for innovation in *ex vivo* cell engineering. Accounts Chem Res 2024. https://doi.org/10.1021/acs.accounts.4c00190.
[29] Lam SJ, O'Brien-Simpson NM, Pantarat N, Sulistio A, Wong EH, Chen YY, Lenzo JC, Holden JA, Blencowe A, Reynolds EC, et al. Combating multidrug-resistant Gram-negative bacteria with structurally nanoengineered antimicrobial peptide polymers. Nature microbiology 2016;1(11):16162. https://doi.org/10.1038/nmicrobiol.2016.162. From NLM.
[30] Qu Y, McGiffin D, Hayward C, McLean J, Duncan C, Robson D, Kure C, Shen R, Williams H, Mayo S, et al. Characterization of infected, explanted ventricular assist device drivelines: the role of biofilms and microgaps in the driveline tunnel. J Heart Lung Transplant 2020;39(11):1289–99. https://doi.org/10.1016/j.healun.2020.07.015. the official publication of the International Society for Heart Transplantation.
[31] Alhmoud H, Delalat B, Ceto X, Elnathan R, Cavallaro A, Vasilev K, Voelcker NH. Antibacterial properties of silver dendrite decorated silicon nanowires. RSC Adv 2016;6(70):65976–87. https://doi.org/10.1039/C6RA13734B. 10.1039/C6RA13734B.
[32] Ivanova EP, Hasan J, Webb HK, Gervinskas G, Juodkazis S, Truong VK, Wu AH, Lamb RN, Baulin VA, Watson GS, et al. Bactericidal activity of black silicon. Nat Commun 2013;4:2838. https://doi.org/10.1038/ncomms3838. From NLM.
[33] Rice KC, Bayles KW. Molecular control of bacterial death and lysis. Microbiol Mol Biol Rev : MMBR (Microbiol Mol Biol Rev) 2008;72(1):85–109. https://doi.org/10.1128/mmbr.00030-07. From NLM.
[34] Chen S, Li L, Zhao C, Zheng J. Surface hydration: principles and applications toward low-fouling/nonfouling biomaterials. Polymer 2010;51(23):5283–93. https://doi.org/10.1016/j.polymer.2010.08.022.
[35] Gómez-Martínez R, Hernández-Pinto AM, Duch M, Vázquez P, Zinoviev K, de la Rosa EJ, Esteve J, Suárez T, Plaza JA. Silicon chips detect intracellular pressure changes in living cells. Nat Nanotechnol 2013;8(7):517–21. https://doi.org/10.1038/nnano.2013.118. From NLM.
[36] Yoh HZ, Chen Y, Aslanoglou S, Wong S, Trifunovic Z, Crawford S, Lestrell E, Priest C, Alba M, Thissen H, et al. Polymeric nanoneedle arrays mediate stiffness-independent intracellular delivery. Adv Funct Mater 2022;32(3):2104828. https://doi.org/10.1002/adfm.202104828.
[37] Elnathan R, Delalat B, Brodoceanu D, Alhmoud H, Harding FJ, Buehler K, Nelson A, Isa L, Kraus T, Voelcker NH. Maximizing transfection efficiency of vertically aligned silicon nanowire arrays. Adv Funct Mater 2015;25(46):7215–25. https://doi.org/10.1002/adfm.201503465.
[38] Chen Y, Alba M, Tieu T, Tong Z, Minhas RS, Rudd D, Voelcker NH, Cifuentes-Rius A, Elnathan R. Engineering micro–nanomaterials for biomedical translation. Adv NanoBiomed Res 2021;1(9):2100002. https://doi.org/10.1002/anbr.202100002.
[39] Chiappini C, De Rosa E, Martinez JO, Liu X, Steele J, Stevens MM, Tasciotti E. Biodegradable silicon nanoneedles delivering nucleic acids intracellularly induce localized in vivo neovascularization. Nat Mater 2015;14(5):532–9. https://doi.org/10.1038/nmat4249. From NLM.
[40] Chen Y, Aslanoglou S, Gervinskas G, Abdelmaksoud H, Voelcker NH, Elnathan R. Cellular deformations induced by conical silicon nanowire arrays facilitate gene delivery. Small 2019;15(47):1904819. https://doi.org/10.1002/smll.201904819.
[41] Qu Y, Daley AJ, Istivan TS, Garland SM, Deighton MA. Antibiotic susceptibility of coagulase-negative staphylococci isolated from very low birth weight babies: comprehensive comparisons of bacteria at different stages of biofilm formation. Ann Clin Microbiol Antimicrob 2010;9(1):16. https://doi.org/10.1186/1476-0711-9-16.
[42] Qu Y, McGiffin D, Kure C, Ozcelik B, Fraser J, Thissen H, Peleg AY. Biofilm formation and migration on ventricular assist device drivelines. J Thorac Cardiovasc Surg 2020;159(2):491–502.e492. https://doi.org/10.1016/j.jtcvs.2019.02.088. From NLM.
[43] Salwiczek M, Qu Y, Gardiner J, Strugnell RA, Lithgow T, McLean KM, Thissen H. Emerging rules for effective antimicrobial coatings. Trends Biotechnol 2014;32(2):82–90. https://doi.org/10.1016/j.tibtech.2013.09.008. From NLM.
[44] Qu Y, McGiffin D, Sanchez LD, Gengenbach T, Easton C, Thissen H, Peleg AY. Anti-infective characteristics of a new Carbothane ventricular assist device driveline. Biofilms 2023;5:100124. https://doi.org/10.1016/j.bioflm.2023.100124. From NLM.
[45] Chandra J, Mukherjee PK, Ghannoum MA. *In vitro* growth and analysis of *Candida* biofilms. Nat Protoc 2008;3(12):1909–24. https://doi.org/10.1038/nprot.2008.192. From NLM.
[46] Marchesan S, Qu Y, Waddington LJ, Easton CD, Glattauer V, Lithgow TJ, McLean KM, Forsythe JS, Hartley PG. Self-assembly of ciprofloxacin and a tripeptide into an antimicrobial nanostructured hydrogel. Biomaterials 2013;34(14):3678–87. https://doi.org/10.1016/j.biomaterials.2013.01.096. From NLM.